

## Nuclear Elastic Scattering of High Energy Protons\*

R. E. RICHARDSON,† W. P. BALL, C. E. LEITH, JR., AND B. J. MOYER

*Radiation Laboratory, Department of Physics, University of California, Berkeley, California*

(Received October 10, 1951)

The differential elastic scattering cross sections of carbon, magnesium, aluminum, silicon, sulfur, copper, silver, tantalum, wolfram, lead, and bismuth for 340-Mev protons are measured as a function of the angle of scattering. The source of the 340-Mev protons is the external scattered deflected proton beam of the Berkeley 184-inch synchrocyclotron. The scattered protons are detected by a triple coincidence scintillation counter telescope whose detection threshold is set by copper energy attenuators placed between the last two trans-stilbene scintillators.

The observed angular distributions are similar to the pattern observed in Fraunhofer diffraction of plane electromagnetic waves by an opaque disk. The details of the diffraction patterns indicate that the nuclei appear partially transparent to the 340-Mev protons.

The observed patterns are found to be consistent with those predicted from elastic scattering of 83-Mev neutrons, indicating that the Coulomb forces are only important in changing the patterns at very small angles.

An attempt is made to observe spin-dependent variations in the patterns from neighboring nuclei whose moments are known to differ appreciably. Within the statistics and resolution of the experiment no appreciable variations are detected.

### I. INTRODUCTION

#### A. Previous Diffraction Experiments

WITHIN certain energy limits elastic scattering of high energy nucleons by nuclei is analogous to optical Fraunhofer diffraction, considering the nucleus as the scattering obstacle and using the DeBroglie wavelength ( $\lambda = h/p$ ) of the high energy nucleons as the incident wavelength.

Amaldi *et al.*<sup>1</sup> have observed the angular distribution of 14-Mev neutrons scattered from Pb nuclei, using neutrons produced by the D+Li reaction. The neutrons had a DeBroglie wavelength of  $7.5 \times 10^{-13}$  cm and were nearly monoenergetic, making them useful for seeking diffraction effects in heavy nuclei. The angular distribution observed had a strong forward peak, with a minimum at about  $25^\circ$  and a small secondary maximum near  $40^\circ$ . Assuming that the Pb nucleus behaved as an opaque sphere, they deduced from the position of the minimum that the radius of the Pb nucleus was about  $1 \times 10^{-12}$  cm.

Using the 90-Mev neutron beam of the 184-inch synchrocyclotron, Bratenahl, Fernbach, Hildebrand, Leith, and Moyer<sup>2</sup> have investigated the diffraction of neutrons by Be, C, Al, Cu, Ag, and Pb. The minima in their patterns were obscured by the energy spread of the neutron beam, which is produced by stripping of 190-Mev deuterons in a one-half inch thick Be target placed in the circulating deuteron beam.<sup>3</sup> The differential scattering cross sections were observed to be not zero in the region of expected secondary maxima for the heavier elements. Their results at the center of the forward

peaks were well described by the opaque nucleus picture, but at larger angles the predictions of the transparent nucleus theory of Fernbach, Serber, and Taylor<sup>4</sup> gave a better fit to the experimental points.<sup>5</sup>

Transparency of a spherical nucleus should alter the shape of the diffraction pattern by increasing the intensity in the region of the minima, decreasing the intensities of the secondary maxima, and causing the entire pattern to broaden slightly corresponding to a slight decrease in radius.

The present experiment makes use of higher energy and better energy resolution, thus providing a better test of the nuclear model. The differential cross sections may be integrated and compared with the total neutron cross sections of DeJuren,<sup>6</sup> and of DeJuren and Moyer.<sup>7</sup> Because of the Rutherford scattering, the proton curves to be integrated must be corrected at small angles in order to compare with neutron results (see Sec. V, B).

#### B. Wavelength of Particles in Present Experiment

Bratenahl *et al.* consider the energy distribution of their neutron beam and the energy dependence of their detection efficiency to arrive at an effective energy of 83 Mev for their particles, giving a DeBroglie wavelength of  $3.05 \times 10^{-13}$  cm. The wavelength of the 340-Mev protons used in the present experiment is  $1.43 \times 10^{-13}$  cm. This shorter wavelength causes the diffraction patterns to be more concentrated in the forward direction, making intensities higher and thus more easily observable above background. The narrowing makes necessary the use of instruments of high angular resolu-

\* This work has been performed under the auspices of the AEC.

† Now at Project Lincoln, M.I.T., Cambridge, Massachusetts.

<sup>1</sup> Amaldi, Bocciairelli, Cacciapuoti, and Trabacchi, *Nuovo cimento* **3**, 15, 203 (1946).

<sup>2</sup> Bratenahl, Fernbach, Hildebrand, Leith, and Moyer, *Phys. Rev.* **77**, 597-605 (1950).

<sup>3</sup> R. Serber, *Phys. Rev.* **72**, 1008 (1947).

<sup>4</sup> Fernbach, Serber, and Taylor, *Phys. Rev.* **75**, 1352 (1949).

<sup>5</sup> It has recently been pointed out by S. Pasternack and H. S. Snyder, *Phys. Rev.* **80**, 921 (1951), that the calculational method may introduce some error into the theoretical curves.

<sup>6</sup> James DeJuren, *Phys. Rev.* **80**, 27 (1950).

<sup>7</sup> J. DeJuren and B. J. Moyer, *Phys. Rev.* **81**, 919 (1951).

tion in order to detect the details of the diffraction pattern.

Protons provide certain distinct advantages over neutrons in such an experiment, namely: (1) a monoenergetic incident beam, (2) exclusion of inelastically scattered particles more easily accomplished by range selection, and (3) detection efficiency essentially unity.

There are a few disadvantages related to the proton charge. Rutherford scattering distorts the diffraction patterns at small angles; but for the energy and scattering thicknesses here employed, this is completely negligible in the region of the detail of interest. Furthermore, the multiple scattering in the target and air path affect angular resolution, and energy loss in the target must be considered.

### C. Nuclear Eccentricities

If the shape of the nucleus is ellipsoidal rather than spherical, and if the nuclei are randomly oriented in the scattering target, the diffraction pattern may be expected to be altered in much the same way as the alteration due to nuclear transparency. Since the nuclear electric quadrupole moment is related to the departure from spherical symmetry, the results of experiments of this type might be used to set upper limits upon the electric quadrupole moments of the nuclei measured. In order to separate the transparency effects from the quadrupole moment effects, the diffraction pattern of a nucleus known to have a high spin is compared with those of its neighbors having spins of zero or one-half. Simple calculation shows that upper limits inferred from experiments of the accuracy here presented would be far larger than the values of eccentricity usually quoted, and greatly improved accuracy would be required to yield any useful information of this sort.

## II. THEORY

### A. Coulomb Correction

The exact solution of the wave equation involving both Coulomb and nuclear force fields is in a series of confluent hypergeometric functions. Since the bombarding energy in this experiment is much higher than the Coulomb barrier energies of the nuclei involved, the effects of the Coulomb field will be neglected as a first approximation. Therefore the theory will be given for the neutron case, with corrections which should come out of the exact solution indicated.

### B. Neutron Solution in Partial Waves<sup>8</sup>

The wave function for the scattered neutron wave, which is obtained by subtracting the expression for the

<sup>8</sup> The method of solution in partial waves was originated by J. W. Strutt (Lord Rayleigh), and presented in Proc. London Math. Soc. (1) IV, 253 (1873), as a method of solution for optical problems. Its application to nuclear physics is presented in most standard texts on wave mechanics. [See for example, Leonard I. Schiff, *Quantum Mechanics* (McGraw-Hill Book Company, Inc., New York, 1949), pp. 103-121.]

unperturbed incident plane wave from the solution for the case in which the scattering nucleus is present, may be represented asymptotically at large distance  $r$  from the scattering center, and at an angle  $\theta$  from the direction of the incident beam by

$$\Psi_{\text{scatt}} \simeq \frac{e^{ikr}}{2ikr} \sum_{l=0}^{\infty} (2l+1)(e^{2i\delta_l} - 1)P_l(\cos\theta), \quad (1)$$

where  $\delta_l$  is determined by matching the solution of the wave equation in the field-free region to that within the boundaries of the scattering potential. If there is no absorption in the scattering nucleus,  $\delta_l$  is a real number measuring the phase shift between the  $l$ th partial wave in the diverging components of the wave function with scatterer present and the corresponding  $l$ th component of the unperturbed plane wave. In the case in which absorption is also present,  $\delta_l$  is a complex number

$$\delta_l = \alpha_l + i\beta_l, \quad (2)$$

where  $\beta_l$  is the exponent determining the absorption of the  $l$ th partial wave.

The  $l$ th partial wave may be associated with particles in the beam which provide an angular momentum of  $l\hbar$  with respect to the center of mass of the system, which is practically the center of mass of the scattering nucleus. Since the wavelength of the incident particles is appreciably smaller than the nuclear radius, it makes sense to speak of the particle colliding within the area represented by the cross section of the nucleus. If the impact parameter is  $b$ , the angular momentum is

$$pb = l\hbar, \text{ from which } l = pb/\hbar = b/\lambda = kb. \quad (3)$$

For the Pb nucleus, values of  $l$  up to nearly  $l=40$  should be considered for 340-Mev particles, since the largest value of impact parameter at which nuclear forces can be felt is equal to  $R$ , the nuclear radius. Particles passing at larger distances should be unaffected, so that no components of the scattered beam should arise from  $l > kR$ .

The corresponding solution for the proton case would contain, besides  $\delta_l$ , an additional phase shift<sup>9</sup>

$$\epsilon_l = \eta_l - \nu \ln 2kr, \quad (4)$$

where  $\nu$  depends upon the charges, masses, and relative velocities of the interacting proton and nucleus, and  $\eta_l$  is the argument of a  $\Gamma$  function which depends upon  $\nu$  and  $l$ . Thus the method of partial waves is not strictly applicable to the proton case, but gives an asymptotic solution independent of  $r$  only for force fields of finite range. The higher values of  $l$  which would be introduced by the Coulomb field give contributions to the cross section only at extremely small angles.

In the opaque nucleus theory it is considered that all particles which strike the nucleus are "absorbed," i.e., removed from the high energy beam by inelastic processes. In this case  $\beta_l$  will be infinite for  $0 \leq l \leq kR$ ,

<sup>9</sup> See reference 8, p. 119.

and zero for  $l$  greater than  $kR$ ; and  $\alpha_l$  is zero for  $l > kR$ . Thus for the perfectly absorbing sphere the scattered wave, Eq. (1), becomes

$$\Psi_{\text{scatt}} \approx -\frac{e^{ikr}}{2ikr} \sum_{l=0}^{l < kR} (2l+1)P_l(\cos\theta). \quad (5)$$

It is interesting to note that these components of the scattered wave are just the corresponding outgoing components of the unperturbed plane wave shifted in phase by  $180^\circ$ . This is equivalent to removing these outgoing components from the total wave field, which is just what would be expected from a perfectly absorbing sphere and is an example of Babinet's principle from physical optics.

The differential scattering cross section per unit solid angle, which is just the square of the amplitude of the scattered wave multiplied by  $r^2$ , is seen to be

$$\frac{d\sigma}{d\Omega}(\theta) = \frac{1}{4k^2} \left[ \sum_{l=0}^{l < kR} (2l+1)P_l(\cos\theta) \right]^2. \quad (6)$$

This distribution may be reduced to the optical Fraunhofer diffraction pattern of plane light waves of wavelength  $\lambda = 2\pi/k$  incident upon an opaque disk of radius  $R' = R + 1/k$ , which is usually given for small angles as

$$\frac{d\sigma}{d\Omega}(\theta) = k^2(R')^4 \left[ \frac{J_1(2kR' \sin \frac{1}{2}\theta)}{2kR' \sin \frac{1}{2}\theta} \right]^2, \quad (7)$$

where  $J_1$  is a first-order Bessel function.

If there is not complete absorption of those particles which strike the nucleus, the problem is one of diffraction of the incident wave by a sphere of material characterized by an index of refraction and an absorption coefficient. The index of refraction is due to the fact that the magnitude of the propagation vector may change within the nucleus because of the nuclear potential well. The absorption coefficient arises from interaction of the incident particle with individual nucleons in the nucleus, which is postulated to be the method of removing particles from the beam by giving rise to inelastic scattering. The absorption coefficient used by Fernbach, Serber, and Taylor<sup>4</sup> is just the numerical density of nucleons in the nucleus multiplied by the nucleon-nucleon scattering cross sections obtained from  $n-p$  and  $p-p$  scattering experiments and modified to allow for the suppression of small momentum transfers in the nucleus due to the Pauli exclusion principle. They obtain for a spherical scatterer with a nonreflecting surface

$$\Psi_{\text{scatt}} \approx \frac{e^{ikr}}{2ikr} \sum_{l=0}^{l+\frac{1}{2} < kR} (2l+1) [e^{(-K+2ik_1)s_l} - 1] P_l(\cos\theta), \quad (8)$$

where  $k_1$  is the change in propagation constant upon entering the nucleus,  $K$  is the absorption coefficient

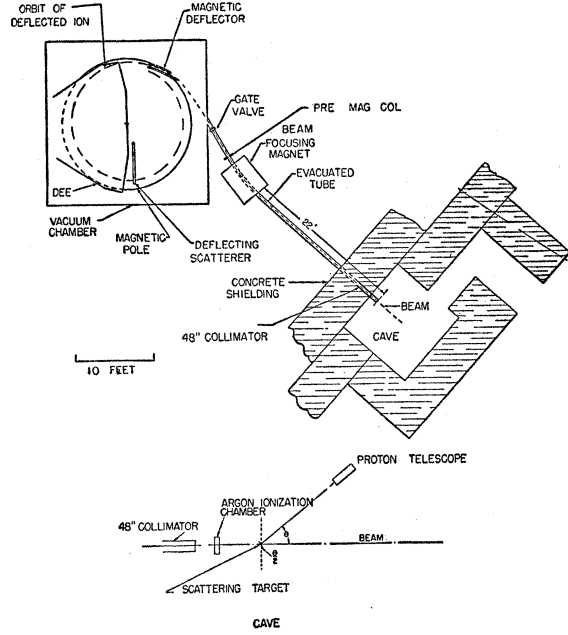


FIG. 1. General arrangement of the experiment.

given by

$$K = (3/4\pi R^3) [Z\sigma_{np}' + (A-Z)\sigma_{nn}'] \quad (9)$$

and  $s_l$  is essentially the path length, within the nucleus, of the particle having angular momentum equal to  $\hbar l$ :

$$s_l = [k^2 R^2 - (l + \frac{1}{2})^2]^{1/2} / k. \quad (10)$$

The criterion for nonreflection is that the potential must not change appreciably within one wavelength.

The cross sections  $\sigma_{np}'$  and  $\sigma_{nn}'$  in Eq. (9) are the effective  $n-p$  and  $n-n$  scattering cross sections for collisions with nucleons in nuclei. In the case of proton diffraction they are replaced by  $\sigma_{pp}'$  and  $\sigma_{np}'$ , respectively. The numerical values to be employed are obtained from known values of  $\sigma_{pp}$  and  $\sigma_{np}$  in free particle collisions, modified by effects of the Pauli principle.

### III. EXPERIMENTAL PROCEDURE

#### A. General Method

In Fig. 1 is shown a diagram of the experimental layout. The collimated external proton beam of the 184-inch synchrocyclotron beam is monitored by an argon-filled ionization chamber whose collected charge is integrated electronically. The scatterer is a thin sheet of material with a cross-sectional area considerably greater than the beam area, and the scattered protons are detected by a triple-coincidence scintillation counter proton telescope which is shielded from particles which may scatter from the mouth of the collimator or from the ionization chamber. The number of incident protons is determined by the charge collected by the ionization chamber, and the number of protons scattered at an

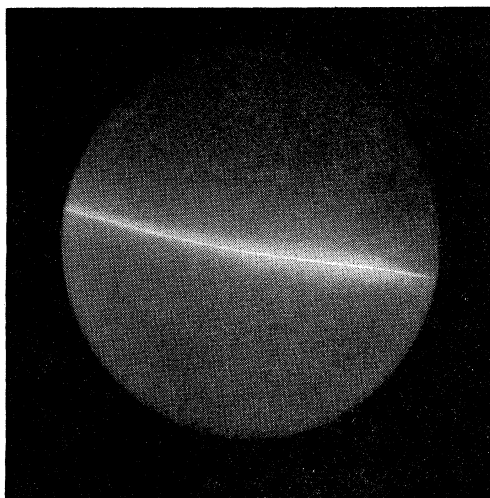


FIG. 2. Autograph of the scattered deflected beam, showing the line character. Made by exposing an x-ray film in the direct beam, positive print, actual size.

angle  $\theta$  into the solid angle offered by the telescope is determined by the number of counts from the telescope. These two numbers may be used to determine the differential scattering cross section, as is shown in Sec. V.

### B. Source of the Proton Beam

When a thin scatterer is placed in the full energy circulating proton beam of the 184-inch synchrocyclotron some of the protons are multiply scattered at such an angle that they enter the magnetic deflecting channel<sup>10</sup> and are removed from the main vacuum chamber into an evacuated tube which carries them through an opening in the main concrete shielding into a separate shielded enclosure usually referred to as the "cave," as shown in Fig. 1. The duration of the scattered beam pulse is about 20  $\mu$ sec with a usual repetition rate of about 60 per second. The energy of the protons which are accepted is determined by the path in the magnetic deflecting channel and by the path through the beam focusing magnet which directs them down the straight portion of the evacuated tube into the cave. The energy of this beam is known from the curvature in the magnetic field, and has also been measured as described below to have a range in Cu of 93.7 g/cm<sup>2</sup> which corresponds to an energy of approximately 340 Mev. The energy may vary by a few Mev from one day to another due to slight differences in the setting up of the deflecting system, but the variation is certainly not more than  $\pm 1$  percent.

### C. Collimation

The beam is collimated to the proper size consistent with the angular resolution desired by means of a 48-

inch long brass plug which is inserted into the evacuated tube where it passes through the 15-foot concrete shielding. For most of the runs, the collimator used had an inside diameter of  $\frac{1}{2}$  inch and was tapered toward the outer end to a diameter of  $\frac{3}{4}$  inch in order to decrease the probability of multiple scattering from the collimator back into the beam. This gives a beam at the scatterer of approximately  $\frac{5}{8}$ -inch diameter. For the high angular resolution runs, the circular collimator in the shielding was replaced by a rectangular collimator in order that the scattered beam might appear to come from a line source instead of a circular source, thus increasing the angular resolution without at the same time introducing too much of a decrease in counting rate.

During the course of this experiment it was discovered that when the premagnet collimator (see Fig. 1) is wide open the cross section of the beam as it enters the cave is concentrated mainly in a line about  $\frac{1}{2}$  inch broad and tilted at an angle of about 13° to the horizontal, as shown in Fig. 2. The rectangular collimator used was  $\frac{3}{16}$  in.  $\times$   $\frac{3}{4}$  in. When it was used, so tilted as to line up with the beam cross section, to replace the  $\frac{1}{2}$ -inch diameter circular collimator, the counting rate was not appreciably changed.

### D. Setting of the Scatterer

In order that all of the protons elastically scattered into the telescope at any given angle will have traversed the same path length and thus have lost the same amount of energy by ionization in the target, the scatterer is not placed perpendicular to the beam, but is inclined to the perpendicular at half the angle by which the telescope is inclined to the beam.

### E. Counting Rate, Background, Accidentals

The triple coincidence counting rate is kept to about one count per beam pulse by controlling the beam intensity. At this counting rate, the number of accidental triple coincidences is negligible, as determined by observing the counting rate as a function of beam intensity. The counting rates in the individual photomultipliers are much higher than this. They are, in fact, sometimes so high that the mechanical registers of the scalers cannot follow them. Since the coincidence unit has a short resolving time, better than the scalers by nearly a factor of a hundred, this high individual counting rate is not objectionable.

After each datum run, a run is made under the same conditions except that the scattering target is removed to determine background. The background is considered in determining the magnitude of the effect as well as in determining the statistical accuracy of the points. The background is comparable to the true counting rate near and after the first minima of the diffraction patterns, necessitating the making of long datum runs and long background runs in order to obtain points of statistical significance in this region.

<sup>10</sup> C. E. Leith, Phys. Rev. 78, 89 (1950).

In order to eliminate any slowly varying instrumental errors such as voltage drift from apparently changing the shape of the diffraction pattern, the datum points are not taken for the angles in numerical order, but are taken at angles much farther apart than the spacing desired in the final points, with the intermediate points taken later.

#### F. Detection Threshold and Absorption by the Energy Attenuators

In order to determine the detection efficiency of the proton telescope and to set the detection threshold, the telescope was placed in the direct beam with no scatterer present, and the counting rate was measured as a function of the thickness of Cu energy attenuator present. For this run, the beam intensity was so low that the argon ionization chamber could not be used as a monitor. Therefore, the double coincidence counts of the first two scintillators, which are before the energy attenuator, were used as a monitor. Because of the thickness of the scintillators and their holders, the curve could not be continued to zero thickness. The curve is shown in Fig. 3, and it is seen that the curve may be extrapolated to a ratio of unity from a thickness corresponding to the Cu equivalent of the scintillators and their dural holders. The curve is seen to cut off at an equivalent thickness of 93.7 g/cm<sup>2</sup> of Cu (mean range), which corresponds to 340 Mev on the curves of Aron, Hoffman, and Williams.<sup>11</sup> The extrapolated range is 95.5 g/cm<sup>2</sup>. Bakker and Segrè<sup>12</sup> have measured the extrapolated range of the electrostatically deflected proton beam to be 93.7 g/cm<sup>2</sup>. Mather<sup>13</sup> has independently determined the energy of the electrostatically deflected beam by means of the Čerenkov radiation in dense glass. He finds the energy to vary from 339 Mev to 341 Mev, depending upon the setting up of the deflecting system. Taking this as a correct value and comparing the range with that of Bakker and Segrè, it is found that the energy of scattered deflected beam may be as high as 344 Mev. It is expected that the scattered deflected beam may have a slightly higher energy than the electrostatically deflected beam, since its orbit must expand to a slightly greater radius than that at which the electrostatic deflector operates. Bakker and Segrè indicate that the curves of Aron *et al.* give an energy which is slightly too low due to the fact that they used too high an ionization potential in their calculations. Since the ionization potential enters into the energy loss equation in a logarithmic term, the error is expected to be small, and the discrepancy between the range-energy curves and the measurements of Mather may be considered to be due to this error.

For most of the data an energy threshold of 330 Mev was employed, while for some of the early runs the value

was 315 Mev. The detection efficiency, which is determined by reading the ratio corresponding to the thickness of energy attenuator used in the experiment, varies from 48 percent to 56 percent in the various runs, but is constant within a given run. In determining the energy threshold, the energy loss of the protons due to ionization in the target must be added to the ionization loss in the counters and energy attenuator; so in the case of a 330-Mev threshold the total copper equivalent of the path to the center of the last crystal was 87.0 g/cm<sup>2</sup>. The decrease in energy due to center-of-mass motion must also be considered, but is negligible except for the lightest target elements used. The decrease in the number of protons due to inelastic scattering in the target of particles which have been elastically scattered is negligible.

#### G. Lining Up the Scattering Frame

The detection angle is determined by setting the pointer of the telescope arm at a particular marker on the calibrated angular scale of the scattering frame. The 0° line is aligned with the proton beam in the following manner:

After the cyclotron has been tuned up and a satisfactory beam has been obtained in the cave, x-ray films are exposed in the beam at the front and rear of the cave. The developed films show darkened spots where the beam has passed through them. The centers of these

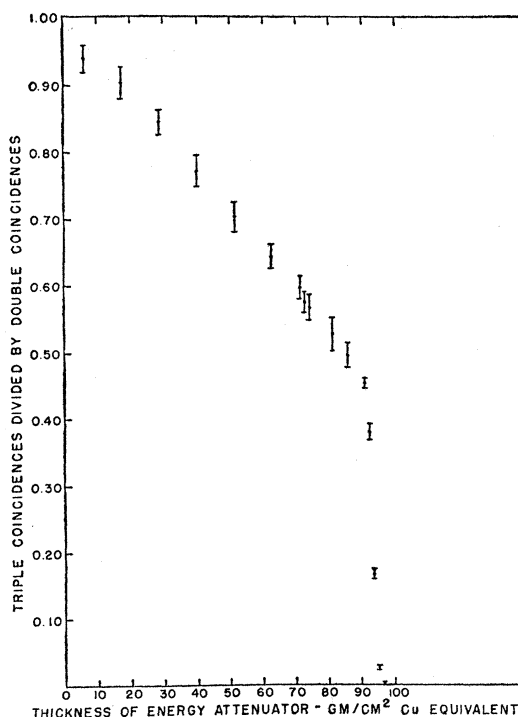


FIG. 3. Energy attenuator effect at zero degrees. The mean range of the beam is 93.7 g/cm<sup>2</sup> of Cu. The extrapolated range is 95.5 g/cm<sup>2</sup> of Cu. Particles are lost in the attenuator both by absorption and by scattering out.

<sup>11</sup> Aron, Hoffman, and Williams, Atomic Energy Commission Unclassified Report No. 663 (1949).

<sup>12</sup> C. J. Bakker and E. Segrè, Phys. Rev. **81**, 489 (1951).

<sup>13</sup> R. L. Mather, Phys. Rev. **84**, 181 (1951).

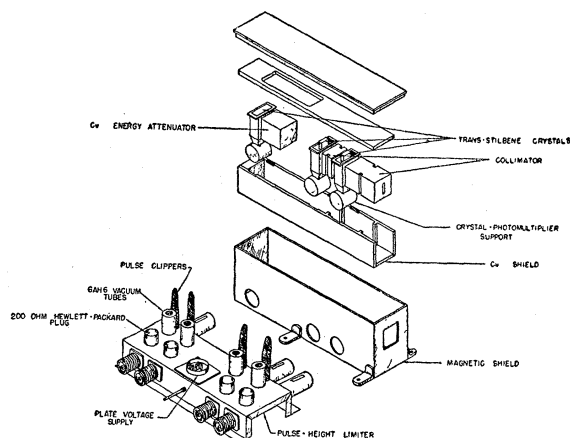


FIG. 4. The proton telescope, showing copper shielding and iron shielding. The energy attenuator is seen before the last crystal holder. The collimating opening may be seen at the front of the telescope. The chassis to the left of the telescope contains pulse-shaping circuits which limit and clip the pulses.

spots are used to stretch a string through the cave in the position occupied by the beam center. Fiducial marks at the front and rear of the scattering frame are then aligned with respect to this string, after which the string is removed, and a film is exposed at the scatterer position as a check on the alignment. With reasonable care, it is possible to align the frame to within a small fraction of a degree.

#### IV. INSTRUMENTATION

##### A. Ionization Chamber and Beam Integrator

The proton beam is monitored with an argon-filled ionization chamber operated at a pressure of 92-cm Hg and with a sensitive thickness of 2.002 inches. The multiplication factor of the chamber has been measured by comparison with a Faraday cage and found to be  $1095 \pm 15$  for 340-Mev protons. The chamber is operated at a voltage high enough so that there is no detectable ion recombination before collection.

The charge collected by the ionization chamber is stored in a standard capacitor whose voltage is continuously recorded upon moving paper tape by means of a Speedomax recorder fed from a feedback dc amplifier. The amplifier maintains its input grid at ground potential so that the leakage in the signal cable leading to the capacitor is negligible and the capacitance of the cable does not have to be considered in determining the total charge collected in terms of the recorded voltage. The recording circuit automatically recycles after attaining a predetermined voltage, and automatically calibrates itself periodically against a standard cell.

##### B. Scatterers

The C, Al, Cu, Ni, and Pb scattering targets were machined from stock materials. The Ta and W targets

were cut from stock foil. The S, Si, and Mg targets are pellets which were compressed from powdered stocks. The Si targets contain a small amount of hydrocarbon binder. The Bi targets were cast. After forming, the targets were weighed on chemical balances and their dimensions measured with micrometer calipers. The weights and dimensions thus determined are used in the calculations. The densities were also calculated and compared with known densities to rule out the possibilities of "blow-holes" or voids.

##### C. Energy Attenuators

The energy attenuators are two-inch square slabs of Cu machined from stock materials. They were weighed and measured in the same manner as were the scattering targets. Their densities were found to agree with the known density.

##### D. Proton Telescope

The scattered protons are detected by a triple-coincidence scintillation counter telescope consisting of three trans-stilbene crystals each viewed by a 1P21 electron photomultiplier tube. The signals from the photomultipliers are amplified, clipped, limited, and fed to the coincidence circuit. It is necessary to limit the amplitude of the pulses since the background includes a great number of inelastically scattered protons which are going slowly in the first two crystals, thus giving pulses very much larger than those due to the elastically

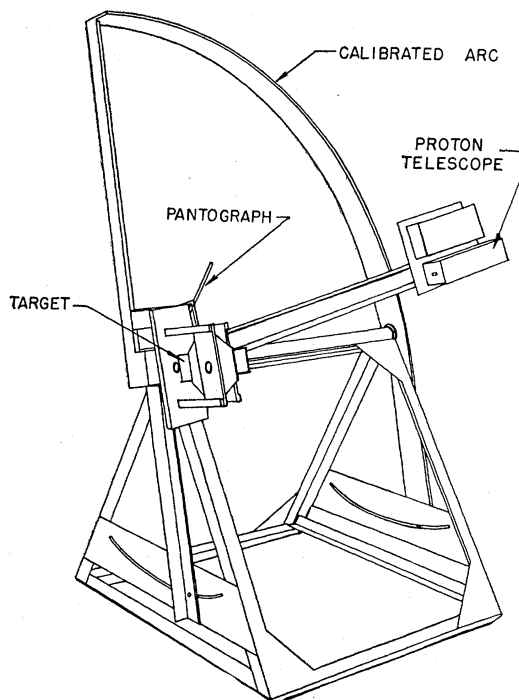


FIG. 5. The tilting proton scattering frame which makes use of the line character of the beam to increase angular resolution without much sacrifice of counting rate.

scattered particles. These large pulses are apt to "feed through" the coincidence circuit unless all the pulses are limited to some standard height. The coincidence circuit is found to work most efficiently when all the pulses are of the order of two volts in amplitude.

The various double coincidence counting rates are measured as a monitor of the operation of the equipment.

Angular resolution of the telescope is determined by the opening in a one-inch thick Cu collimating block placed between the first and second phosphors. This thickness is sufficient so that any particle missing the opening will not be counted in the last crystal.

In order to decrease the individual counting rates the entire telescope is enclosed in a  $\frac{1}{4}$ -inch thick Cu box to keep out the general background of "slow" particles which exists in the cave. In front of the first crystal is placed a three-inch long Cu block having in it a hole of the same size as the hole in the collimating block. It has been determined that the presence of this block appreciably decreases the single counting rates of the first and second phosphors by keeping out randomly directed particles.

The first and second phosphors are made only slightly larger than the opening in the collimating block since the ambient background counting rate is dependent upon the whole volume of the scintillators, while only the portion offered to the collimator is effective in giving true counts. The last crystal is made approximately an inch and a half square in order to count a large portion of the protons which are multiply scattered in the energy attenuating Cu blocks.

The stray magnetic field in the cave due to the cyclotron magnet is about 20 gauss. Since photomultipliers may be affected by this field, the entire telescope, except for an entrance hole, is enclosed in a magnetic shield of one-eighth inch thick mild steel with a  $\frac{1}{4}$ -inch thick lid. The proton telescope is shown in Fig. 4.

### E. Scattering Frame

The scattering frame is shown in Fig. 5. It is so constructed that the plane in which the measurements are made may be set perpendicular to the "line source" which the beam produces as it strikes the scatterer. The scattering targets are mounted upon a remotely controlled hexagonal wheel allowing several targets to be run at the same scattering angle without necessitating a shutdown of the cyclotron in order to enter the cave. Pilot lights at the control station indicate which target is in the scattering position at any time.

The proton telescope is clamped to a rigid Dural channel which keeps it pointed at the scatterer. This arm is pivoted upon the shaft which supports the scatterer wheel. The four-inch by  $\frac{3}{8}$ -inch Dural plate which makes up the circular arc of the frame is calibrated at one degree intervals, and the arm, which carries a vernier calibrated in tenths of a degree, may be clamped to the circular arc at any angle.

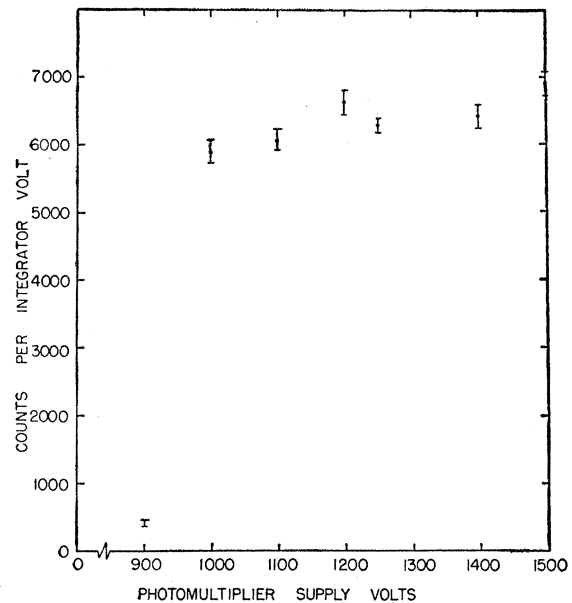


Fig. 6. Typical voltage plateau for the detecting system with 340-Mev protons incident.

In order that the target will always be set at half the angle at which the telescope is set, the scatterer support is connected to the telescope arm by means of an equal-arm pantograph, which insures bisection of the angle.

### F. Coincidence Circuit

The coincidence circuit used in this experiment is a Rossi type quadruple coincidence circuit using a crystal diode as a diode clamp in the plate circuit, and a crystal diode signal expander circuit in the output. It was designed and constructed at this laboratory by R. Madey and B. Ragent for use in meson experiments, and is very similar to one devised by Garwin.<sup>14</sup> In order to use this as a triple coincidence circuit, the signal from one of the photomultipliers is split and fed into two different channels of the coincidence circuit. The resolving time is approximately  $2 \times 10^{-8}$  second. The signals from the photomultipliers, after shaping, are amplified by Hewlett-Packard type 460-A distributed amplifiers before being fed to the coincidence circuit, and the coincidence output is fed through a linear amplifier to a scaler.

In order to insure that all of the protons scattered into the telescope are counted, a check is made of counting rate as a function of the photomultiplier tube supply voltage. As the voltage is increased it is expected that more of the weak pulses will be made large enough to cause counts. At excessively high tube voltages, the thermal noise level is expected to be so high as to give accidental coincidences. In Fig. 6 is shown a typical plot of triple coincidence counts per unit integrated beam as a function of tube voltage. It is seen that there is a very

<sup>14</sup> R. L. Garwin, Rev. Sci. Instr. 21, 569 (1950).

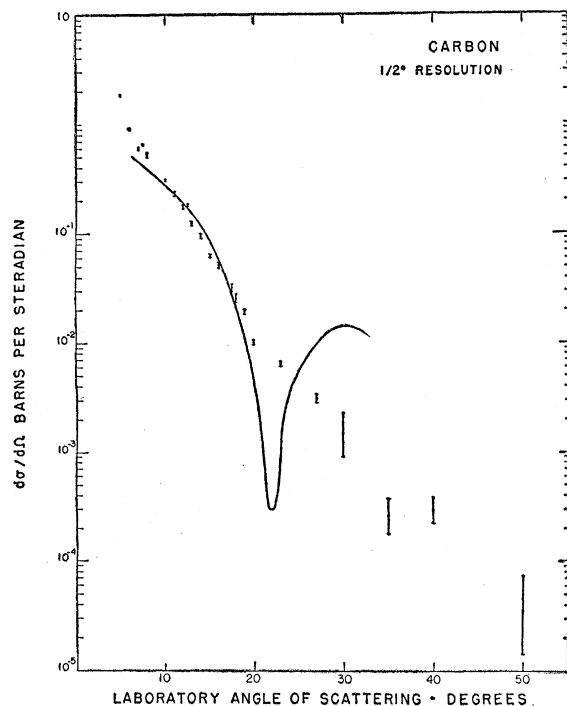


FIG. 7. Differential elastic scattering cross section as a function of angle for 340-Mev protons on C. The curve is the prediction of the transparent nucleus theory, modified for the effect of the finite angular resolution.

broad plateau in which all of the protons are being counted, but accidental coincidences are negligible.

## V. CALCULATIONS

### A. Differential Scattering Cross Section

If the cross section does not vary appreciably over the angular region accepted by the telescope, at a given nominal angle, the number of true counts expected in the proton telescope when  $n$  protons are incident is given by

$$K(\theta) = NnT_a(d\sigma/d\Omega)\Delta\Omega, \quad (11)$$

where  $N$  is the number of scattering nuclei per square centimeter;  $n$  is the number of incident protons, which is measured by the ionization chamber, with known multiplication factor;  $T_a$  is the transmission factor of the energy attenuator and telescope, which is varied from 0.48 to 0.56 for the various runs;  $\Delta\Omega$  is the solid angle subtended by the proton telescope; and  $d\sigma/d\Omega$  is the differential elastic scattering cross section. It must be noted that  $N$  varies as  $(\cos\frac{1}{2}\theta)^{-1}$  since the target is turned through  $\frac{1}{2}\theta$ . Solution for  $d\sigma/d\Omega$  yields the values presented in Sec. VI.

The true counting rate is determined from the actual data by subtracting the background counts per integrator volt from the actual counts per integrator volt recorded during a datum run. The statistical deviation due to the counting statistics is the square root of the

sum of the squares of the individual deviations of actual and background counts per volt.

### B. Total Cross Section for Elastic Scattering

The total elastic scattering cross section is found by integrating the differential cross section over all angles. While the measurements do not give a true picture of nuclear scattering at very small angles, due to Coulomb effects, the total solid angle included in these angles is very small. As an approximation for the integration, the differential cross-section curve is made to approach the zero degree axis in the same manner as would be inferred from the 83-Mev neutron results of Bratenahl *et al.*<sup>2</sup> The contributions at angles larger than those measured will be less than 1 percent.

### C. Angular Resolution

The angular resolution is determined by the geometry of the detection system and by the thickness of the scattering target. The size of the beam at the target, which determines the effective size of the source which the telescope sees, and the size of the opening in the telescope collimating block are so chosen that the maximum deviation from the nominal scattering angle at which a proton may be scattered and still be detected is equal to the nominal angular resolution. The angular deviation at which the intensity falls to half-maximum is somewhat smaller than this. The angular spread due to multiple Coulomb scattering in the target is Gaussian, with the thicknesses of the targets so chosen that the

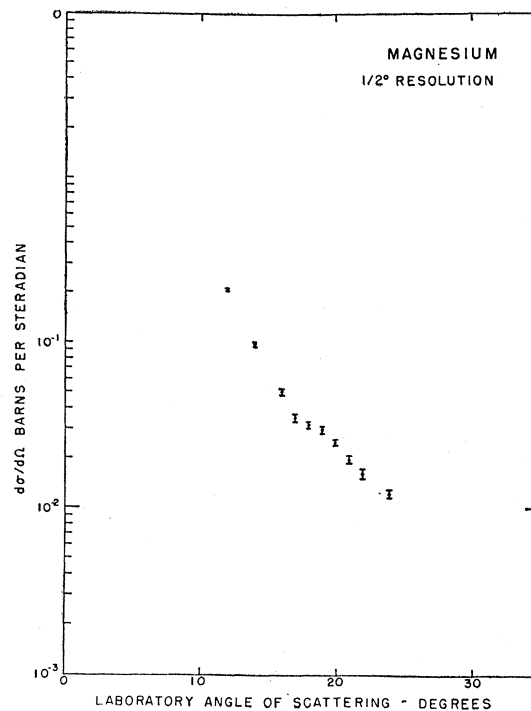


FIG. 8. Differential elastic scattering cross section as a function of angle for 340-Mev protons on Mg.

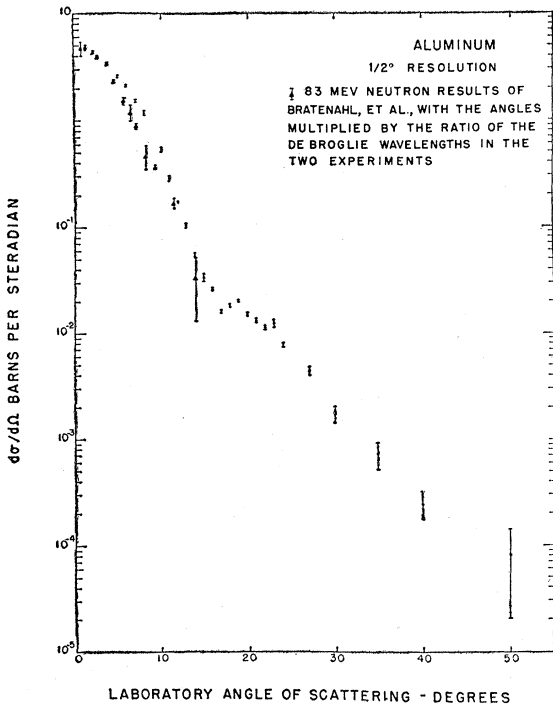


FIG. 9. Differential elastic scattering cross section as a function of angle for 340-Mev protons on Al.

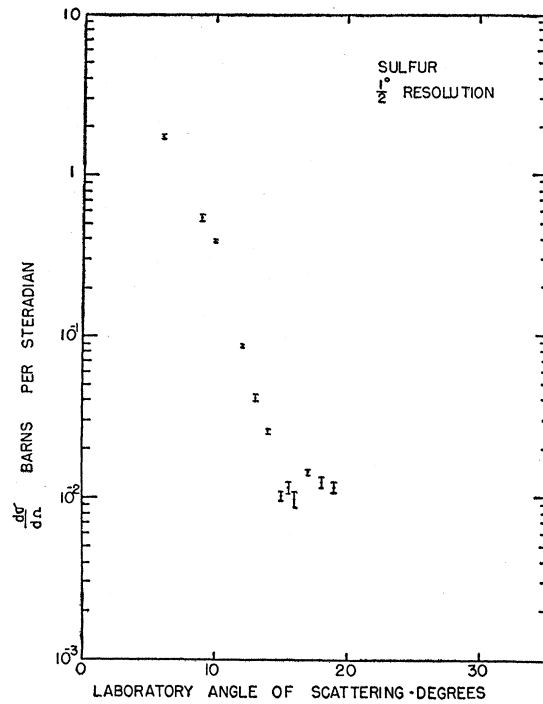


FIG. 11. Differential elastic scattering cross section as a function of angle for 340-Mev protons on S.

half-width at half-maximum is equal to the nominal angular resolution. The angular divergence of the incident beam is negligible in the determination of angular

resolution, due to the long path from the cyclotron to the cave.

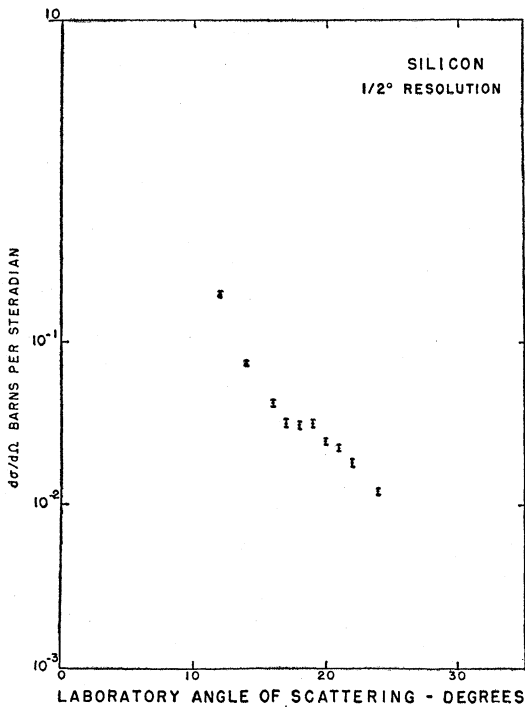


FIG. 10. Differential elastic scattering cross section as a function of angle for 340-Mev protons on Si.

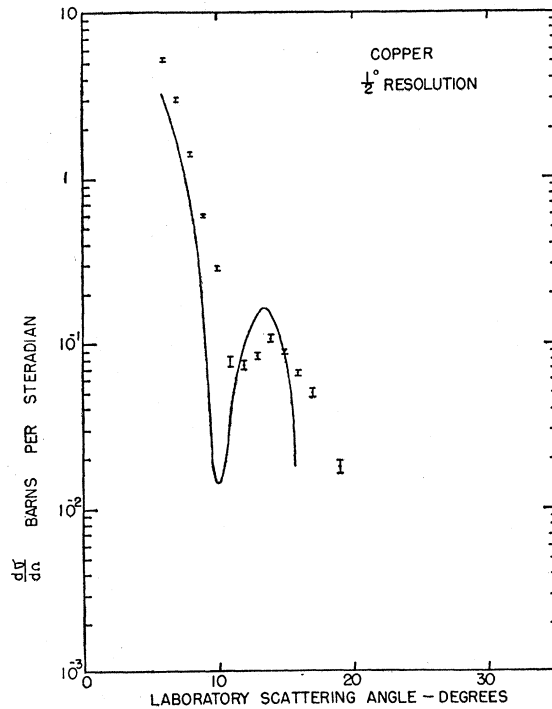


FIG. 12. Differential elastic scattering cross section as a function of angle for 340-Mev protons on Cu. The curve is the prediction of the transparent nucleus theory, modified for the effect of the finite angular resolution.

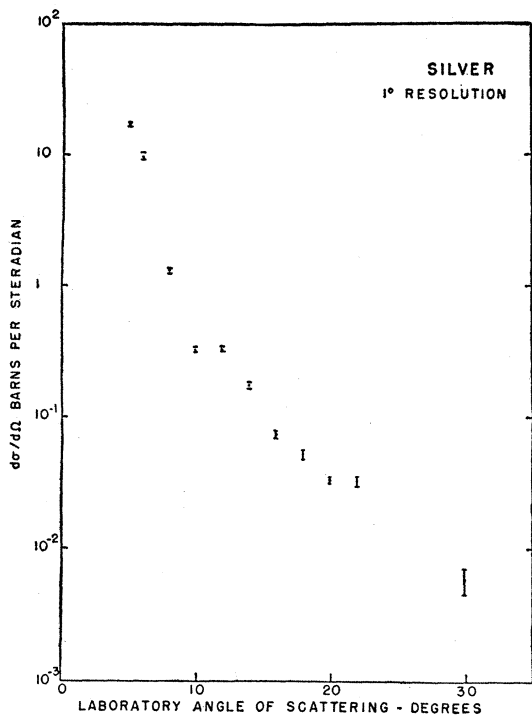


Fig. 13. Differential elastic scattering cross section as a function of angle for 340-Mev protons on Ag.

The total air path of the protons from the exit of the evacuated tube to the telescope is two meters. The root-mean-square displacement of 340-Mev protons in this

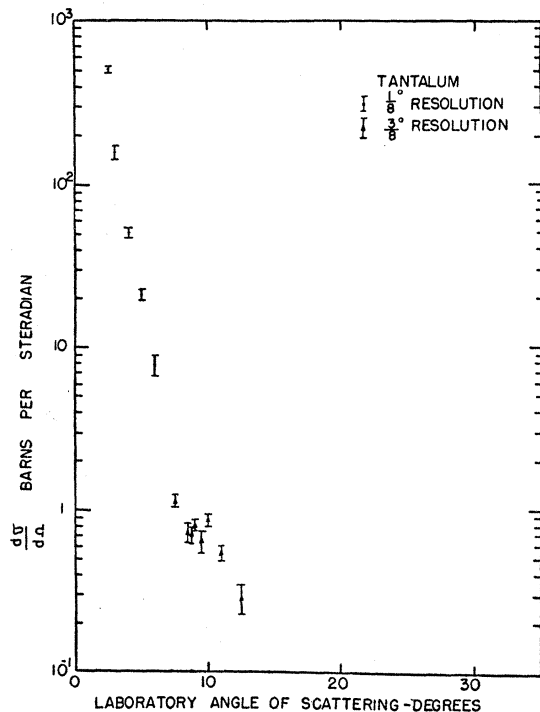


Fig. 14. Differential elastic scattering cross section as a function of angle for 340-Mev protons on Ta.

path length is 1.8 mm. This displacement at the telescope would correspond to an angular spread of approximately  $\pm 0.1^\circ$ .

## VI. RESULTS AND CURVES<sup>15</sup>

### A. Angular Distributions

The data for the angular distributions for the elements measured are plotted in Figs. 7 through 17. The differential elastic scattering cross section in barns per steradian is shown as a function of the angle of scattering in the laboratory system, which is equivalent to the center-of-mass system except for large angles where the difference is a few degrees for light elements. The center-of-mass angle is larger than the laboratory angle by  $3.5^\circ$  at  $50^\circ$  for C. The difference is only  $1.6^\circ$  for Al at  $50^\circ$ . It is correspondingly smaller for the heavier elements. The errors shown are the usual standard deviations based upon counting statistics.

Because of the large variation of the cross sections with angle, the cross-section scale is made logarithmic. It is interesting to note that the ratio of the differential cross section of C at  $5^\circ$  to that at  $50^\circ$  is about 60,000. It should be noted that the data are not all plotted with the same scales.

The curves shown are the predictions of the transparent nucleus theory, modified for the effect of finite angular resolution. On the Al curve, the datum points of Bratenahl *et al.* have been plotted, with the angle multiplied by 0.469, which is the ratio of the wavelengths in the two experiments.

In Fig. 18 the positions of the maxima and minima of the measured diffraction patterns are plotted as a function of atomic mass number. The apparent tendency of the lower mass points to lie above an  $A^{1/3}$  curve is to be expected from transparent nucleus concepts.

### B. Total Elastic Scattering Cross Sections

The total cross sections for "nuclear" elastic scattering are found by continuing the curves toward zero degrees in the same shape as was found in the neutron case by Bratenahl *et al.* The resulting curves are then integrated to determine the total elastic scattering cross sections. The results are tabulated in Table I.

## VII. SOURCES OF ERROR

### A. Detection of Inelastically Scattered Particles

Cladis, Hadley, and Moyer<sup>16</sup> are investigating the protons scattered by nucleon-nucleon collisions when 340-Mev protons impinge upon various target nuclei. The description of this type of scattering is fairly well supplied by simple two-body collision considerations in which the target nucleon has an initial momentum characteristic of a particle in a nucleus. This simple

<sup>15</sup> Preliminary results have been given by Richardson, Ball, Leith, and Moyer, Phys. Rev. **83**, 859 (1951).

<sup>16</sup> Cladis, Hadley, and Moyer, Phys. Rev. **81**, 649 (1951).

picture is of course only an approximation in view of the requirements imposed by the final state of the residual nuclear system and over-all conservation of energy.

In the small-angle region this process will contribute some protons with energies above the threshold of the proton telescope. Their number is, however, sufficiently small as to be insignificant in data of the accuracy here presented, except possibly in the case of carbon in the vicinity of  $5^{\circ}$ - $10^{\circ}$ .

In this connection it should be mentioned that some of the early runs were made with a 315-Mev threshold, and their results were not significantly different from those made with the 330-Mev threshold.

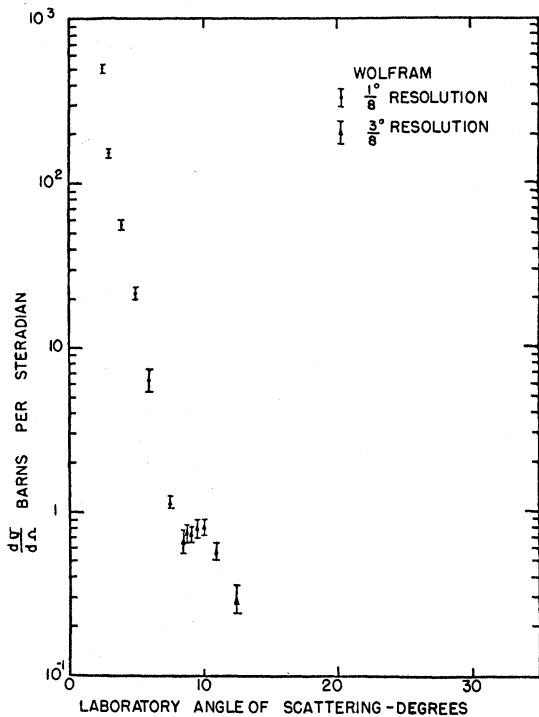


FIG. 15. Differential elastic scattering cross section as a function of angle for 340-Mev protons on W.

**B. Energy Threshold**

It is not possible to determine exactly the detection threshold of the apparatus because of straggling in the energy attenuator. For convenience, the same energy attenuator is used in most of the runs having the same angular resolution. The energy loss in the scatterers, which were chosen so as to have multiple scattering angles appropriate to the angular resolution desired, varied by a few Mev. This means that the detection threshold was not exactly the same for all elements, but the variation was so small as to be unimportant. The same energy attenuator was used for all angles. Since the correction for center-of-mass motion is small, the variation of energy of elastically scattered protons with angle is relatively unimportant. As an extreme example, the

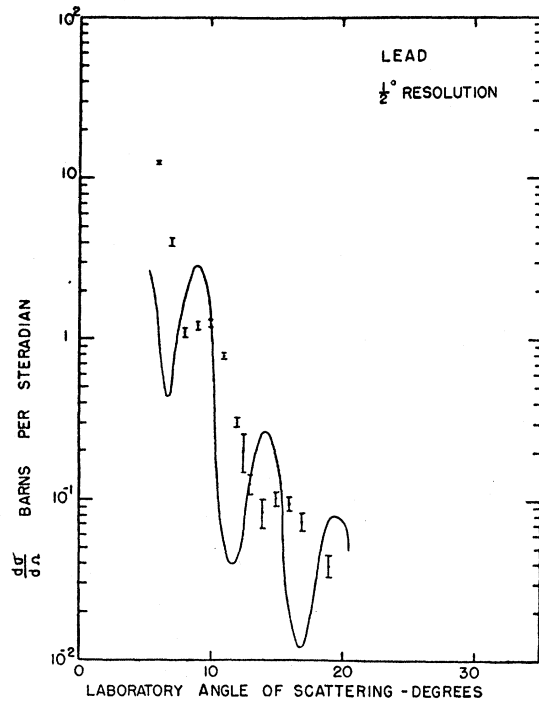


FIG. 16. Differential elastic scattering cross section as a function of angle for 340-Mev protons on Pb. The curve is the prediction of the transparent nucleus theory, modified for the effect of the finite angular resolution.

energy decrease due to center-of-mass correction is only about 5 Mev for C at  $30^{\circ}$ . Nearly all of the datum points

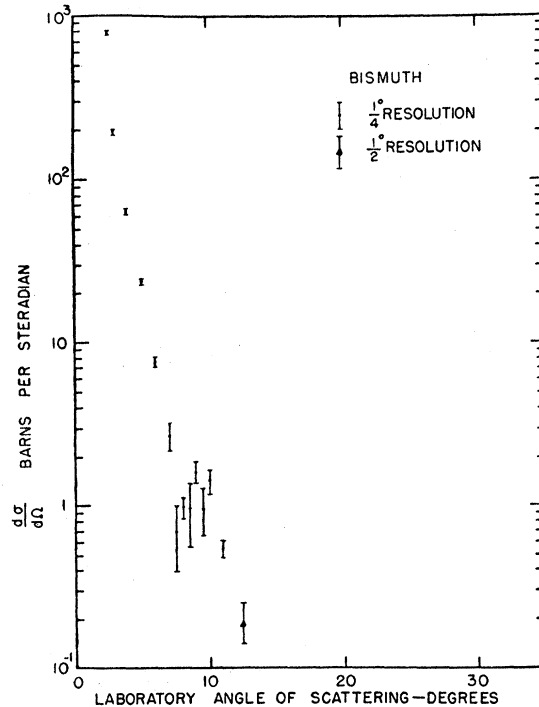


FIG. 17. Differential elastic scattering cross section as a function of angle for 340-Mev protons on Bi.

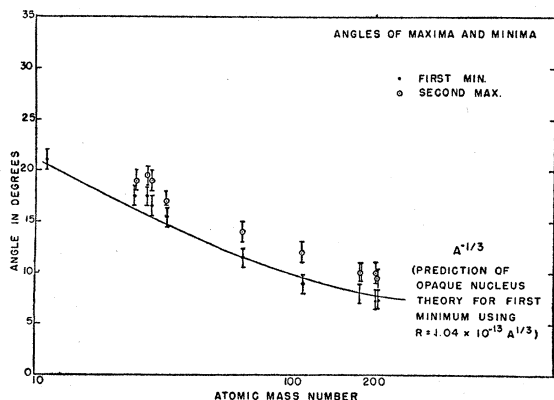


Fig. 18. Angles of maxima and minima plotted vs atomic mass number.

included in this paper are at smaller angles than this, where the effect is not even this large.

### C. Double Scattering in Target

An uncertainty not yet considered is the possibility of a proton experiencing two wide-angle scattering events in the target. The probability for a double scattering into an angle  $\theta$  is proportional to the product of the probability of scattering into an angle  $\alpha$  and that for scattering into  $\beta$ , where  $\theta = \alpha + \beta$ . This is negligible for the thin targets and for the angles considered.

### D. Rutherford Scattering into Large Angles

Williams<sup>17</sup> has considered relativistic Coulomb scattering and has corrected for the finite size of the nucleus, considering the charge to be uniformly distributed throughout the nucleus. He obtains for the differential scattering cross section

$$\frac{d\sigma}{d\Omega}(\theta) = \left[ \frac{Ze^2}{2M\beta^2c^2\gamma} \right]^2 \frac{1}{\sin^4 \frac{1}{2}\theta} \frac{1}{\left[ 1 + \left( \frac{b}{\lambda} \sin \frac{1}{2}\theta \right)^2 \right]^2} \quad (12)$$

where all symbols have their usual meaning, with  $M$

TABLE I. Total cross sections for "nuclear" elastic scattering.<sup>a</sup>

Element	Cross section (barns)
C	0.098
Al	0.201
Cu	0.515
Ag	0.884
Pb	0.934

<sup>a</sup> No errors are indicated, since the value is very sensitive to the method of continuing the differential cross sections toward zero degrees. In some cases, the use of the datum points at very small angles instead of neglecting the Coulomb scattering by continuing the curves to match the corresponding neutron data would change the cross section by a factor of 2 or 3. The value shown is in each case less than the upper limit set by the work of DeJuren (see reference 6) and DeJuren and Moyer (see reference 7) for 270-Mev neutrons.

<sup>17</sup> E. J. Williams, Proc. Roy. Soc. (London) 169A, 531 (1939).

being the reduced mass. This formula gives cross sections of  $6.7 \times 10^{-25}$  cm<sup>2</sup> and  $7.9 \times 10^{-26}$  cm<sup>2</sup> at 6° and 8°, respectively, from Pb. These cross sections are down by a factor of about thirty from the values measured in this experiment. For C at 10° the factor is greater than one hundred.

Gatha<sup>18</sup> is at present undertaking the solution of the wave equation including both the Coulomb and nuclear effects and considering transparency. His preliminary results indicate that the Coulomb effect should be important only up to about 2° for C and 6° for Pb.

It is interesting to set an approximate upper limit upon the angle at which a proton may scatter by single Rutherford scattering. The maximum sidewise momentum which the proton may acquire in the collision is proportional to the square root of the Coulomb barrier energy of the struck nucleus. The square root of the ratio of the barrier energy to that of the total kinetic energy (incident energy) will then give an approximate upper limit to the angle. For 340-Mev protons incident upon Pb, this angle is about 12°, while for C it is about 5°.

The angular distribution of multiply Coulomb scattered particles is Gaussian. The probability for multiple Coulomb scattering into an angle greater than twice the half-width at half-maximum of the Gaussian is less than the probability for single Rutherford scattering into the same angle, which has been shown to be negligible.<sup>17</sup>

## VIII. CONCLUSIONS AND COMPARISON WITH THEORY

### A. Angular Distributions

The angular distributions are seen to give evidence of diffraction as expected, except for C. It is even possible to suspect a minimum for C near 20°, but the datum points are not close enough together to make the minimum certain. Since the transparent nucleus theory considers a model in which the nucleus is a sphere with an index of refraction, the model probably does not hold for such a light nucleus with its small number of nucleons. The results of this experiment indicate that C appears quite "open" to the 340-Mev protons.

The relative heights of the secondary maxima of succeeding orders agree favorably with diffraction theory for Pb in which two secondary maxima have been observed. The minima appear at slightly larger angles than in the theoretical curves, indicating that the nuclei are probably even more transparent than assumed in the transparent nucleus theory.

The 83-Mev neutron results may be matched by a nuclear radius given by  $R = 1.39 \times 10^{-13} A^{\frac{1}{3}}$  cm. If the nuclear radii are calculated by Eq. (7), using the positions of the first minima found in this experiment, it is found that the radii of opaque nuclei which would give

<sup>18</sup> K. M. Gatha, private communication.

minima at those positions would be given by a coefficient which varies from 0.84 for C to 1.13 for Pb. This is again an indication of nuclear transparency.

### B. Total Cross Sections for Elastic Scattering

The total cross sections for nuclear scattering, omitting the Coulomb part, were determined by counting squares on a curve of cross section per unit angle  $d\sigma/d\theta = 2\pi \sin\theta d\sigma/d\Omega$ , plotted as a function of angle. Although the total solid angle offered at large angles is much greater than that at small angles, the cross sections fall off rapidly enough that the contribution for angles greater than  $30^\circ$  is negligible in all cases. The results of the integration are consistent with the neutron results in that they fall always below the upper limits for elastic scattering indicated by the neutron experiments.

### C. Nuclear Eccentricities

The high spin nuclei show no statistically important differences from their zero-spin neighbors, except that the Al minimum appears slightly sharper, but the resolution is such that nuclear eccentricities would need to be much larger than currently held values to be discernible.

### IX. ACKNOWLEDGMENTS

The authors wish to express their gratitude to Professor E. O. Lawrence for his kind interest in the progress of this work. They also wish to thank the cyclotron crew and especially Mr. J. L. MacMullen for their assistance in the investigation of the structure of the emergent proton beam. Dr. S. Fernbach and Dr. K. M. Gatha have been very helpful in discussions of the theoretical aspects.

## Nuclear Photodissociation by High Energy Synchrotron Gamma-Rays\*

SEISHI KIKUCHI

*Cornell University, Ithaca, New York*

(Received October 15, 1951)

The stars and single proton tracks produced in photographic emulsions exposed to a beam of high energy synchrotron gamma-rays have been analyzed. The maximum energy of the bremsstrahlung spectrum was varied between 150 and 300 Mev. The following subjects were studied: 1. the cross section for star production as a function of the excitation energy; 2. the energy distribution of the protons from stars as well as single protons; 3. the angular distribution of star protons as well as single protons; and, 4. the relative number of stars associated with a meson coming out.

The cross section for the nuclear photoevents increases with increasing energy above the meson threshold. There seem to be two sorts of processes taking place in competition with each other. One is the so called free meson effect; namely, a free meson is

produced inside the nucleus by the interaction of a photon with a nucleon and is then absorbed in the same nucleus. The other effect is a process in which a photon is absorbed directly by a group of nuclear particles without emitting a real meson. Evidence for the free meson effect is seen in the fact that the angular distribution of star protons of energy between 20 and 60 Mev in the case of 300-Mev excitation shows a strong forward peak. Evidence for the existence of the direct absorption of photons comes from the fact that the angular distribution of star protons of high energy, say about 100 Mev, shows a forward asymmetry.

The cross section for direct absorption is much larger than expected from Levinger's theory of nuclear photodissociation. The cross section should be at least of the same order of magnitude as the free meson effect.

### I. INTRODUCTION

NOT much is known about the photodissociation of nuclei by gamma-rays whose quantum energy is above the threshold of photomeson production. The cross section for  $(\gamma, n)$ ,  $(\gamma, p)$ ,  $(\gamma, 2n)$ ,  $(\gamma, np)$ ,  $\dots$  reactions has been studied up to about 100 Mev, and the results show that the cross sections reach their maximum somewhere below 50 Mev and then decrease gradually to a very small value, which is not yet exactly measured. The purpose of the present experiment is to investigate the nuclear photodissociation when the energy of the photon exceeds the meson threshold, by studying the stars and the single proton tracks produced in a photographic emulsion exposed directly to a beam of high energy synchrotron gamma-rays.

It is expected that above the meson threshold stars will be produced by the emission and subsequent absorption of mesons in the same nucleus. Actually, it was found that the probability for star production begins to increase as the energy of the photon exceeds the meson threshold.<sup>1</sup> The problem is whether or not this effect can be explained in terms of the so called free meson effect alone. The present results indicate not only the existence of the free meson effect but the existence of another effect whose cross section is comparable with the free meson effect.

The production of high energy protons from any target irradiated by high energy gamma-rays has been reported, and their energy distribution and angular

\* This work has been supported by the ONR.

<sup>1</sup> R. D. Miller, Phys. Rev. **82**, 260 (1951); S. Kikuchi, Phys. Rev. **81**, 1060 (1951).

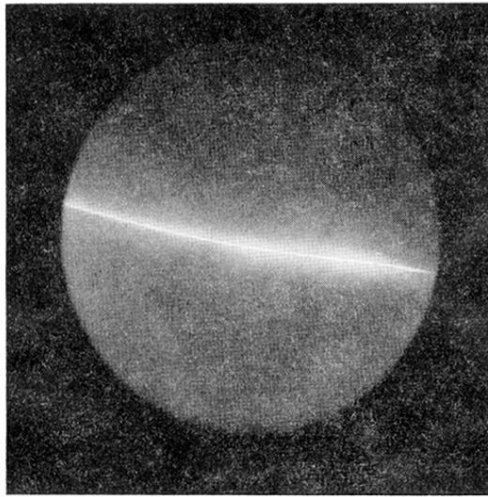


FIG. 2. Autograph of the scattered deflected beam, showing the line character. Made by exposing an x-ray film in the direct beam, positive print, actual size.